Metamaterials with negative permeability and permittivity: Analysis and Applications

José Manuel Tapadas Alves

***Abstract*—In this work we study and analyse the electromagnetic phenomena of media with a negative permeability and permittivity, called DNG metamaterials, and how it leads into some physical phenomena such as the appearance of backward waves and the emergence and implications of negative refraction. Two simple DNG waveguiding structures are also studied: the DPS-DNG interface and the DNG slab. As a DNG medium is necessarily dispersive, the utilization of a known dispersive model, the Lorentz Dispersive Model, is used in the analysis of the DPS-DNG interface, in order to obtain physical significative results. The appearance of super-slow modes in the DNG slab propagation is also a subject of analysis. Finally we address the study of lens design using DNG metamaterials. The dependence on the refractive index of this design process is evidenciated. The particular structure of the DNG Veselago's flat lense is also analyzed in order to study a potentially practical application of DNG metamaterials in optics and the implications of dealing with such materials, as this lens structure overruns some conventional limitations allowing propagating waves to be brought to single point focus producing an image that has sub-wavelength detail.**

***Index Terms*—Double Negative Media, Metamaterials, Negative Refraction, Backward Waves, Planar Waveguides, Lens Design, Superlens, Microwaves, Photonics**

I. Introduction

WITH the introduction of these new physical propreties of DNG metamaterials, the study and interpretation of the associated results is in fact very attractive and challaging. There are many established physical concepts that must be re-interpreted in order to comply with this new paradigm and there is also the probability of finding new effects associated with this kind of materials, since there is a whole new set of resulting physical phenomena. In this work we have the possibility to associate and consolidate the more conventional and well known electromagnetic concepts but now, with the introduction of the DNG metamaterials, in a more generalized perspective, as we study the physical effects found even on simple guiding structures. As up to today the demonstrations and experiments of the new physical phenomena associated with DNG metamaterials have lead to the construction of new types of microwave structures whose applications to mobile communication systems have attracted a lot of attention from the scientific community. These metamaterials could help improve the performance of several communication devices, such as antennas, and a lot of effort is being made on the the design of antennae using this kind of periodic structures. This kind of material also have implications on lens design. The main objective of this work is the analysis and study of wave propagation in DNG metamaterial guides, and also the application of this kind of materials in lens design, taking advantage of its particular electromagnetic properties to achieve results that are not present in conventional lenses. We try to understand the new physical phenomena that are associated with double negative media and the effects when applied to well known propagation guide structures. The study of lens design using DNG materials is also addressed in order to verify the different results between these kind of lens against the physical limitations of common DPS lenses.

II. Electromagnetics of Double Negative (DNG) Media

LET us consider a specific material that is characterized by the two electromagnetic macroscopic constitutive parameters: the electrical permittivity ε and the magnetic permeability μ. The permittivity and the permeability are often treated as complex functions of the frequency of the applied field, since complex numbers allow the specification of magnitude and phase [1].

$$\varepsilon = \varepsilon' + \varepsilon'' \tag{1}$$

with $\varepsilon', \varepsilon'' \ \epsilon \ \Re$. And:

$$\mu = \mu' + \mu'' \tag{2}$$

with $\mu', \mu'' \ \epsilon \ \Re$

Figure 1 shows the location of each medium qualification in a diagram whose axis is formed by $\varepsilon' = \Re(\varepsilon)$ and $\mu' = \Re(\mu)$.

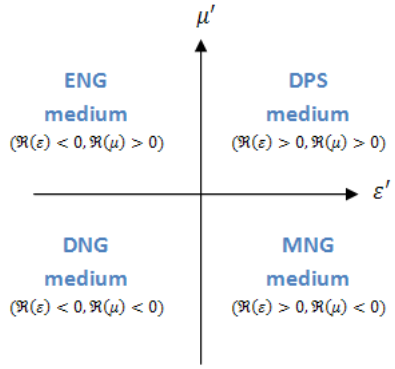

Figure 1. Material Classification

We can write the expressions for both the electric and magnetic fields in the time and z-axis domain:

$$\mathbf{E} = \widehat{x} E_0 \exp[i(kz - \omega t)] \tag{3}$$

$$\mathbf{H} = \widehat{y} H_0 \exp[i(kz - \omega t)] \tag{4}$$

Where the complex wave number **k**, is given by:

$$\mathbf{k} = k\widehat{z} \tag{5}$$

The vacuum wave-number k_0, is given by:

$$k_0 = \omega\sqrt{\varepsilon_0 \mu_0} = \frac{\omega}{c} \tag{6}$$

where c is the speed of light. Now we can define the frequency dependant refraction index n from (5) and (6) :

$$n = \sqrt{\mu\varepsilon} \tag{7}$$

The polarization does not respond instantaneously to an applied field. Taking this into consideration, we can define a complex refraction index:

$$n = n' + in'' \tag{8}$$

where n' is the refractive index indicating the phase velocity coefficient and $n^{''}$ is called the **extinction coefficient**, which indicates the amount of absorption loss when the electromagnetic wave propagates through the material. Both n' and n'' are dependent on the frequency [1]. Let us now define, based on (8) and (5), the **phase velocity** v_p, of an electromagnetic wave:

$$v_p = \frac{\omega}{\Re(k)} = \frac{\omega}{k_0 \Re(n)} = \frac{c}{n'} \tag{9}$$

We can now write the complex amplitude equations for both the electric and the magnetic field using (8):

$$\mathbf{E} = \widehat{x} E_0 \exp[ink_0 z] = \widehat{x} E_0 \exp[-n'' k_0 z] \exp[in' k_0 z] \tag{10}$$

$$\mathbf{H} = \widehat{y} \frac{E_0}{\zeta \eta_0} \exp[ink_0 z] = \widehat{y} \frac{E_0}{\zeta \eta_0} \exp[-n'' k_0 z] \exp[in' k_0 z] \tag{11}$$

The Time-Average Poynting Vector, is given by:

$$\mathbf{S}_{av} = \frac{1}{2} \Re(\mathbf{E} \times \mathbf{H}^*) \tag{12}$$

Using the expressions (10) and (11) on (12) we obtain:

$$\mathbf{S}_{av} = \widehat{z} \frac{|E_0|^2}{\eta_0} \Re\left[\frac{1}{\zeta}\right] exp[-2n'' k_0 z] \tag{13}$$

In this case the value of n'' needs to be always positive in order to verify energy extinction along with the propagation of the wave on the z-axis, as expected since we are dealing with a passive media where:

$$\lim_{z \to \infty} |\mathbf{E}| \leq E_0 \tag{14}$$

As we can see from (13) it depends on the sign of the real part of the normalized impedance's value. We have:

$$\Re\left[\frac{1}{\zeta}\right] = \Re\left[\frac{n}{\mu}\right] = \Re\left[\frac{n' + in''}{\mu' + i\mu''}\right] = \frac{n'\mu' + n''\mu''}{\mu'^2 + \mu''^2} \tag{15}$$

As we have seen above, we are dealing with a passive media, so, as we concluded from (14), we have:

$$n'' > 0 \rightarrow k'' > 0 \rightarrow \mu^{''}, \varepsilon^{''} > 0 \tag{16}$$

In (7) we have established a relation between the refraction index and both the permittivity and permeability, so we will use that in order to infer about the nature of $n^{'}$.

$$n = n_\mu n_\varepsilon = \sqrt{\mu}\sqrt{\varepsilon} \tag{17}$$

We will now study the permittivity ε in the complex plan using polar coordinates.

$$\varepsilon = \rho_\varepsilon \exp[i\theta_\varepsilon] \tag{18}$$

We can also define the permittivity dependent part of the refraction index in polar coordinates:

$$n_\varepsilon = \sqrt{\varepsilon} = n_\varepsilon^{'} + in_\varepsilon^{''} = \sqrt{\rho_\varepsilon} \exp\left[i\frac{\theta}{2}\right] \tag{19}$$

As we are dealing with a passive DNG media ($\varepsilon^{'} < 0$ and $\varepsilon^{''} > 0$) we have for θ_ε:

$$\theta_\varepsilon = \left[\frac{\pi}{2}, \pi\right] \tag{20}$$

We can also define n_ε by:

$$n_\varepsilon = \sqrt{\varepsilon} = n_\varepsilon^{'} + in_\varepsilon^{''} = i(n_\varepsilon^{''} - in_\varepsilon^{'}) = i\rho_\varepsilon \left[\sin\left(\frac{\theta_\varepsilon}{2}\right) - i\cos\left(\frac{\theta_\varepsilon}{2}\right)\right] \tag{21}$$

And from (20) we can obtain the argument of n_ε (by dividing it by 2):

$$\frac{\theta_\varepsilon}{2} = \left[\frac{\pi}{4}, \frac{\pi}{2}\right] \tag{22}$$

From (22) we now that for this specific interval both $\cos\left(\frac{\theta_\varepsilon}{2}\right)$ and $\sin\left(\frac{\theta_\varepsilon}{2}\right)$ must be greater than 0 so we must choose the positive root. Knowing this and with (19) we can now write:

$$n_\varepsilon^{'} = \sqrt{\frac{|\varepsilon'|}{2}} \sqrt[4]{1 + \left(\frac{\varepsilon''}{\varepsilon'}\right)^2} \sqrt{\frac{1 + sgn(\varepsilon')}{\sqrt{1 + \left(\frac{\varepsilon''}{\varepsilon'}\right)^2}}} \tag{23}$$

$$n_\varepsilon^{''} = \sqrt{\frac{|\varepsilon'|}{2}} \sqrt[4]{1 + \left(\frac{\varepsilon''}{\varepsilon'}\right)^2} \sqrt{\frac{1 - sgn(\varepsilon')}{\sqrt{1 + \left(\frac{\varepsilon''}{\varepsilon'}\right)^2}}} \tag{24}$$

We know that we are dealing with DNG media so $sgn(\varepsilon^{'}) = -1$. We can now easily see by the result in (23) and (24) , and for the interval that we have defined for $\frac{\theta_\varepsilon}{2}$, that $n_\varepsilon^{''} > n_\varepsilon^{'}$.

Let us now consider the limit case where there are no losses, from (23) and (24) we obtain:

$$n_\varepsilon^{'} = 0 \tag{25}$$

$$n_\varepsilon^{''} = \sqrt{|\varepsilon'|} \tag{26}$$

And with these results in (25) and (26) we can write:

$$n_\varepsilon = i\sqrt{|\varepsilon'|} \tag{27}$$

$$n_\mu = i\sqrt{|\mu'|} \tag{28}$$

With these two last results and using the definition in (17) we can now easily obtain the refraction index for a DNG media:

$$n = n_\mu n_\varepsilon = i\sqrt{|\mu'|} i\sqrt{|\varepsilon'|} = -\sqrt{|\mu'\varepsilon'|} \tag{29}$$

As we have seen from (23) and (24), $n_\varepsilon^{''} > n_\varepsilon^{'}$ and the same happens for the permeability as the demonstration process is analogous so $n_\mu^{''} > n_\mu^{'}$, resulting in:

$$n^{'} = -(n_\varepsilon^{''} n_\mu^{''} - n_\varepsilon^{'} n_\mu^{'}) < 0 \tag{30}$$

$$n^{''} = (n_\varepsilon^{'} n_\mu^{''} + n_\varepsilon^{''} n_\mu^{'}) > 0 \tag{31}$$

The results in (30) and (31) are indeed very important because they not only corroborate the result in (16) that states that there is an extinction of the field along the propagation axis (as $n^{''} > 0$) but it also gives us the final conclusion about the direction of the power flux since $n^{'} < 0$ so from (13) and (15) we can say that:

$$\mathbf{S} \cdot \widehat{z} > 0 \tag{32}$$

As $n^{'} < 0$ we can also state from (9) that we are dealing with medium with **negative phase velocity** as its direction is the opposite from the energy flow and attenuation, from (32). In polar coordinates we have:

$$n = \sqrt{\rho_n}\exp(i\theta_n) = \sqrt{\rho_\varepsilon}\sqrt{\rho_\mu}\exp\left[i\frac{\theta_\varepsilon + \theta_\mu}{2}\right] \tag{33}$$

We saw that the condition was valid for n_ε and n_μ the argument was in the interval $\left[\frac{pi}{4}, \frac{pi}{2}\right]$ so it is easy to see from (33) that $arg(n)$ is also between those values. The refraction index on a DNG medium is in fact negative and we can now relate it with the propagation constant:

$$\mathbf{k} = k \cdot \widehat{z} = nk_0 \cdot \widehat{z} = \widehat{z}(n^{'}k_0 + in^{''}k_0) \tag{34}$$

As $n^{'}k_0 < 0$ we can see that the direction of propagation is the opposite compared with the energy flux:

$$k^{'} \cdot \widehat{z} < 0 \tag{35}$$

From (32) and (35) we can create a graphical representation, in Figure 2, of both the electric and magnetic fields with the energy flux vector and the propagation constant for a DPS medium and for a DNG medium and compare the results:

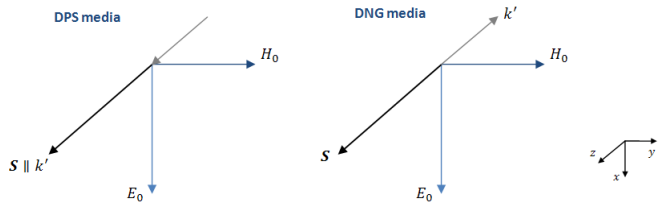

Figure 2. Spatial Representation of the fields, the energy flux and the propagation constant for a DPS and a DNG medium

These are the designated **Backward Waves [2]**, electromagnetic waves that present a propagation direction that is the opposite of the associated power flux. Let us now consider the scattering of a wave that incises on a DPS-DNG interface as shown in Figure 3.

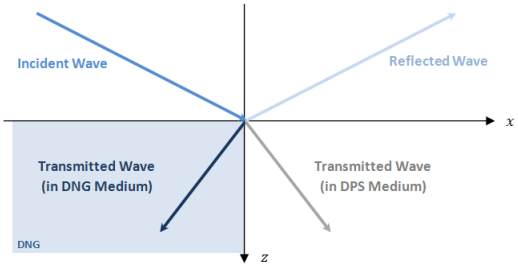

Figure 3. Scattering of a wave that incises on a DPS-DNG interface

The **Snell's law of reflection** assures us that the angle of reflection is equal to the angle of incidence:

$$\theta_r = \theta_i \tag{36}$$

If we consider an uniform plane wave incising obliquely on a plane boundary (z=0) between materials with different constitutive parameters (and refraction indexes n_1, n_2), and enforcing the boundary conditions at the interface, we can also obtain, from the Snell's law of reflection which is given by:

$$\frac{\sin(\theta_t)}{\sin(\theta_i)} = \frac{n_1}{n_2} \tag{37}$$

If we now consider the situation represented by the previous , where there is a DNG material with a negative refraction index n_2 we see that, for obtaining the correct angle of the transmitted wave one must write (37) in the following form:

$$\theta_t = sgn(n_2)\arcsin\left[\frac{n_1}{|n_2|}\sin(\theta_i)\right] \tag{38}$$

We must note that if the refraction index of a medium is negative, according the Snell's Law, the refracted angle should also become "negative" and then, as we have seen in the previous section, the direction of the energy flux, given by **S**, is the opposite of the wave propagation, given by **k**. The expression for the time-averaged energy density of a plane wave is:

$$\mathcal{U} = \frac{1}{4}\left[\varepsilon_0\frac{\partial(\omega\varepsilon)}{\partial\omega}|\mathbf{E}|^2 + \mu_0\frac{\partial(\omega\mu)}{\partial\omega}|\mathbf{H}|^2\right] \tag{39}$$

If we multiply by μ and ϵ and then add them together we obtain the following expression, that we will call $\mathcal{A}$, which will be usefull further in this section:

$$\mathcal{A} = 2\mu\varepsilon + \omega\left[\mu\frac{\partial(\omega\varepsilon)}{\partial\omega} + \varepsilon\frac{\partial(\omega\mu)}{\partial\omega}\right] \tag{40}$$

Since we are dealing with a DNG medium, where $\varepsilon, \mu < 0$, we can conclude that $\mathcal{A} < 0$.

For an isotropic medium we have:

$$\mathbf{k}^2 = \omega^2\mu_0\mu\epsilon_0\epsilon \tag{41}$$

Deriving it in order of the frequency ω we obtain:

$$\frac{\partial(\mathbf{k}^2)}{\partial\omega} = \mu_0\varepsilon_0\omega\mathcal{A} \tag{42}$$

So we can also write:

$$\frac{\partial(\mathbf{k}^2)}{\partial\omega} = 2\mathbf{k}\frac{\partial(\mathbf{k})}{\partial\omega} = 2nk_0\frac{\partial(\mathbf{k})}{\partial\omega} = 2\mathbf{n}\frac{\omega}{c}\frac{\partial(\mathbf{k})}{\partial\omega} \tag{43}$$

We obtain:

$$\frac{\partial(\mathbf{k}^2)}{\partial\omega} = 2\omega\frac{1}{v_p}\frac{1}{v_G} \tag{44}$$

Since $\mathcal{A} < 0$ this implies that $\frac{\partial(\mathbf{k}^2)}{\partial\omega} < 0$ and knowing that for a lossy DNG medium we have a negative phase velocity, we can conclude that, on a dispersive DNG medium, the group velocity and the phase velocity have diferent signs. For dispersive media is also easy to prove that the group velocity and phase velocity have diferent values (since for a non-dispersive media $v_p = v_G$). We obtain:

$$\frac{\partial(\mathbf{k})}{\partial\omega} = \frac{\partial(\omega\mathbf{n})}{\partial\omega}\frac{1}{c} = \frac{1}{c}\left(n + \omega\frac{\partial\mathbf{n}}{\partial\omega}\right) \tag{45}$$

We can now write:

$$\frac{1}{v_G} = \frac{1}{v_p} + \frac{1}{c}\omega\frac{\partial\mathbf{n}}{\partial\omega} \tag{46}$$

That shows us that $v_p = v_G$ is only possible when there is no frequency dependance of the refraction index.

Figure 4. The plannar interface between a DPS and a DNG medium, here represented by a dashed line.

III. Guided Wave Propagation in DNG Media

A. Propagation on a DPS-DNG Interface

In this section we will study the propagation of electromagnetic waves on a plannar interface between a DPS and a DNG medium, which is represented in Figure 4.

The sign of the propagation constant $h_i = i\alpha_i$ is chosen in such way that the field decays with distance away from the interface so the resulting fields on both the DPS and DNG regions (that we will call **1** and **2** respectively). Admiting that the interface is on $x = 0$, the field's expressions are given by:

$$\mathbf{E}_y(x) = \begin{cases} E_0 \exp[-\alpha_1 x] & , x > 0 \\ \\ E_0 \exp[\alpha_2 x] & , x < 0 \end{cases} \tag{47}$$

With α_1 , α_2 > 0.

We can now use Faraday's Law, from the Maxwell Equations, to compute the magnetic field:

$$\nabla \times \mathbf{E} = -i\omega\mu\mathbf{H} \tag{48}$$

From Eq. (48) we can now obtain the expressions for the magnetic field on both regions:

$$\mathbf{H}_z(x) = \begin{cases} \frac{E_0\alpha_1}{i\omega\mu_1} \exp[-\alpha_1 x] & , x > 0 \\ \\ \frac{-E_0\alpha_2}{i\omega\mu_2} \exp[\alpha_2 x] & , x < 0 \end{cases} \tag{49}$$

Aplying the boundary conditions at the interface ($x = 0$), and assuring the continuity of the magnetic field components ($H_z(0)^- = H_z(0)^+$) we can write the modal equation for the **Tranverse Magnetic** (TM) propagation mode given by:

$$\alpha_2\mu_1 + \alpha_1\mu_2 = 0 \tag{50}$$

By aplying a simillar computation process to both the wave equation and field expressions for the TM modes, and using the following equation from the Maxwell Equations:

$$\nabla \times \mathbf{H} = \omega\varepsilon\mathbf{E} \tag{51}$$

We can also obtain the modal equation for the TE mode:

$$\alpha_2\varepsilon_1 + \alpha_1\varepsilon_2 = 0 \tag{52}$$

With these results we are now able to infere if there is propagation along the interface. Since we now that both $\alpha_1, \alpha_2 > 0$ and $\mu_1, \varepsilon_1 > 0$, from (52) :

$$\alpha_1 = -\frac{\mu_1}{\mu_2}\alpha_2 > 0 \Longrightarrow \mu_2 < 0 \tag{53}$$

And from (52):

$$\alpha_1 = -\frac{\varepsilon_1}{\varepsilon_2}\alpha_2 > 0 \Longrightarrow \varepsilon_2 < 0 \tag{54}$$

So, from the implications on (53) and (54), we can conclude that it is in fact possible to have propagation on an interface between a DPS medium and a DNG medium (ε_2, $\mu_2 < 0$). We will now use the Lorentz Dispersive Model (LDM)for the frequecy dependant permittivity and permeability:

$$\varepsilon_{r,L}(\omega) = 1 + \frac{\omega_{pe}^2}{i\omega\Gamma_L + \omega_{0e}^2 - \omega^2} \tag{55}$$

$$\mu_{r,L}(\omega) = 1 + \frac{\omega_{pm}^2}{i\omega\Gamma_L + \omega_{0m}^2 - \omega^2} \tag{56}$$

This model will be used to describe the frequency dependance of the parameters on the DNG medium (region **2**), and have choosen the following values for the plasma's frequencies ω_{pm}, ω_{pe}, central frequencies ω_{0e}, ω_{0m}, damping coefficient Γ_L, as well as the parameters of the DPS medium $\varepsilon_{1,r}$, $\mu_{1,r}$. The simulation parameteres are represented at Table 2.1.

Parameter	Value
ω_{pe}	$2\pi \times 7 \times 10^9 rad.s^{-1}$
ω_{pm}	$2\pi \times 6 \times 10^9 rad.s^{-1}$
ω_{0e}	$2\pi \times 2.5 \times 10^9 rad.s^{-1}$
ω_{0m}	$2\pi \times 2.3 \times 10^9 rad.s^{-1}$
Γ_L	$-0.05 \times \omega_{pe}$
$\varepsilon_{1,r}$	1
$\mu_{1,r}$	1

Table I
Simulation parameters for the Lorentz Dispersive Model, on the DPS-DNG interface structure

The constitutive parameters are graphically represented in Figure 5.

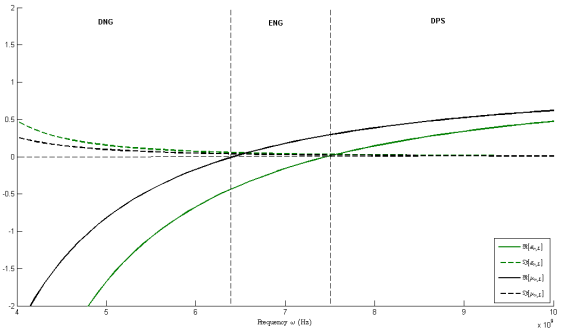

Figure 5. Lorentz dispersive model for $\varepsilon_{r,L}$ and $\mu_{r,L}$

From 5 we can identify that the three regions: DNG, ENG and DPS. The positive imaginary parts are the result of a "negative" damping present on the Lorentz's Model.

A representation of the refraction index can be obtained and is shown in Figure 6.

In Figure 6, as we expected, on the DNG region we have a negative refraction index and on the DPS region we have a positive refraction index. From the variation n on the ENG region, where we also have a negative real component of the refraction index, we can take an important conclusion. The existance of a negative real refraction index on this ENG region proves that a DNG medium has always the designation of (Negative Refraction Index) but a NRI medium does not have to be DNG, as we can see when considering losses and dispersion. The representation of the dispersion relation, $\beta(\omega)$ is showed in Figure 7.

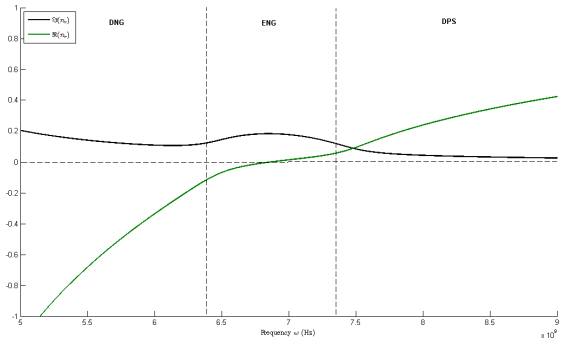

Figure 6. Relative refraction index ($n_r = \frac{n}{\sqrt{\varepsilon_0 \mu_0}}$), using the lossy LDM, on the DPS-DNG interface.

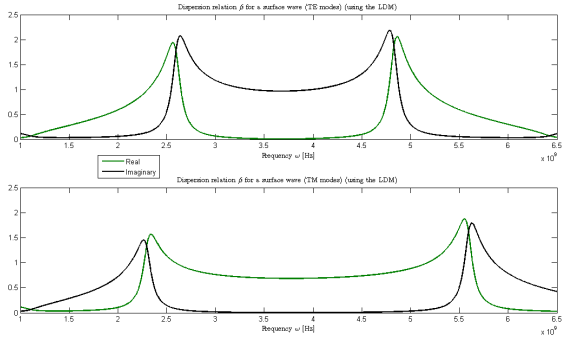

Figure 7. Dispertion relation, $\beta(\omega)$, using the lossy LDM, on the DPS-DNG interface.

Both the real and the imaginary parts of $\beta(\omega)$ experience a significative increase in the range of frequencies where there were asymptotes ($\left|\frac{\mu_2(\omega)^2}{\mu_1^2}\right| = 1$ (or $\left|\frac{\varepsilon_2(\omega)^2}{\varepsilon_1^2}\right| = 1$) but they can now represent valid physical solutions as the propagation constant is no longer infinite. The representation of the attenuation constants for both the TE and TM modes are depiced in Figure 8 and Figure 9.

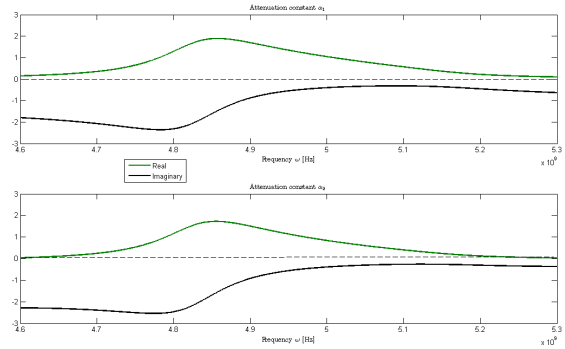

Figure 8. Atenuattion constants α_1 and α_2, for the TE modes, using the lossy LDM, on the DPS-DNG interface

The attenuation constants have also, for this frequency interval, a positive real part, as a condition to have propagation along the interface and exponential atenuation as we move away from it, as stated in (53) and (54) but now the imaginary parts of both α_1 and α_2 are always negative, condition that is needed in order to have propagation along the z-axis. From the expressions in (47) we can

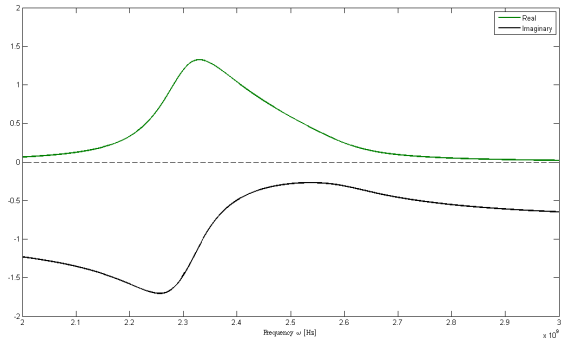

Figure 9. Atenuattion constants α_1, for the TM modes, using the lossy LDM, on the DPS-DNG interface

also have a graphical representation of the electric field's variation along the x-axis dimension. This is shown in Figure 10. The variation of the field shows us that the field intensity increases as we aproach $x = 0$, as we expected, because this is a representation of the field in the interface (which is at $x = 0$) and the attenuation as we get further from it. From modal equations (50) and (52) we can also verify that the solpe of the field branches is also influentiated by the values of both the permittivities and the permeabilities of the DPS and DNG media.

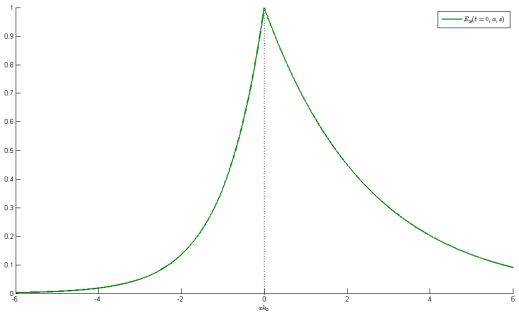

Figure 10. Variation of the electric field, $E_y(t = 0, x, z)$, on the DPS-DNG Interface

B. Propagation on a DNG slab

In this section we will study the propagation of electromagnetic waves on a DNG slab waveguide represented by Figure 11 :

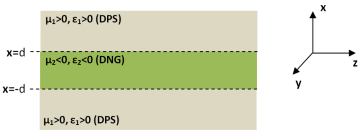

Figure 11. A DNG slab waveguide immersed on a DPS media

For the TE modes we have the following wave equation:

$$\frac{\partial^2}{\partial x^2}\mathbf{E} + \left(k_0^2 n_i^2 - \beta^2\right)\mathbf{E} = 0 \tag{57}$$

The solutions form this equation, considering that $-d < x < d$, can take the form of:

$$E_y = A\cos(h_1 x) + B\sin(h_1 x) \tag{58}$$

with $h_1 = \omega^2\mu_1\varepsilon_1 - \beta^2$.

For this structure we have presented for the slab, we want that the electric field decays with distance as we get away from the slab, so the evanescence of the electric field can be represented by:

$$\mathbf{E}_y(x) = \begin{cases} C\exp(jh_2x) & , x \geq d \\ \\ D\exp(jh_2x) & , x \leq -d \end{cases} \tag{59}$$

Where the transverse wave number is defined by:

$$h_2 = \pm j\alpha_2 \tag{60}$$

With the attenuation constant, α_2, given by:

$$\alpha_2^2 = \beta^2 - k_2^2 = \beta^2 - \omega^2\varepsilon_2\mu_2 \tag{61}$$

Placing this attenuation constant in (59) we can now establish for the evanescent fields the following expressions:

$$\mathbf{E}_y(x) = \begin{cases} C\exp(-\alpha_2x) & , x \geq d \\ \\ D\exp(\alpha_2x) & , x \leq -d \end{cases} \tag{62}$$

From the result on (59) we can see that there are two kinds of solutions:

- one even solution, given by the $\cos(h_1x)$ term,
- one odd solution, given by the $\sin(h_1x)$ term.

We can now represent the electric field, inside and outside the slab, by the following relations:

$$\mathbf{E}_y(x) = \begin{cases} B\sin(h_1x)\exp(-j\beta z) & , |x| \leq d \\ \\ C\exp(-\alpha_2x)\exp(-j\beta z) & , x \geq d \\ \\ D\exp(\alpha_2x)\exp(-j\beta z) & , x \leq -d \end{cases} \tag{63}$$

Obtaining the magnetic field expression can be done by using Faraday's Law, from the Maxwell's Equations:

$$\nabla \times \mathbf{E} = -i\omega\mu\mathbf{H} \tag{64}$$

Applying this equation on the resultant field expression on (63) we obtain the magnetic field for this structure. Applying the boundary conditions at the interface ($x = d$), assuring the continuity of the magnetic field components $\widehat{z}$, and assuming that $B = A = E_1$ and $C = D = E_2$, we can achieve the results for the both the odd and even TE modal equations for the slab structure:

$$\begin{cases} -h_1d\frac{\mu_2}{\mu_1}\cot(h_1d) = \alpha 2d & \text{(Odd Modes)} \\ \\ h_1d\frac{\mu_2}{\mu_1}\tan(h_1d) = \alpha 2d & \text{(Even Modes)} \end{cases} \tag{65}$$

Using the same procedure to obtain the TM modes we get:

$$\begin{cases} -h_1d\frac{\varepsilon_2}{\varepsilon_1}\cot(h_1d) = \alpha 2d & \text{(Odd Modes)} \\ \\ h_1d\frac{\varepsilon_2}{\varepsilon_1}\tan(h_1d) = \alpha 2d & \text{(Even Modes)} \end{cases} \tag{66}$$

We can now simplify the modal equations by making the following substitutions:

$$a = \alpha_2 d \tag{67}$$

$$b = h_1 d \tag{68}$$

The relation between the normalized propagation's constants is given by:

$$a^2 + b^2 = V^2 \tag{69}$$

Where V, the normalized frequency, is given by:

$$V = k_0 d\sqrt{\varepsilon_2\mu_2 - \varepsilon_1\mu_1} \tag{70}$$

The intersection of the curve (70) with the modal equations will represent the modal solutions for these modes in the slab.

We will now study the surface modes on the DNG slab. From (62) we can easily find that the transverse propagation constant h_1 can take real values if $\beta < \omega\sqrt{\varepsilon_1\mu_1}$ and imaginary values if $\beta > \omega\sqrt{\varepsilon_1\mu_1}$ and, for the analysis of the slab, we know that assuming either imaginary or real values for h_1 we will maintain the surface mode conditions where we have the wave diminish with distance from the slab. Let us now assume that $B = -ib$, if we consider that $\tan(ix) = i\tanh(x)$ and $\cot(ix) = -i\coth(x)$ we can now rewrite equations (69) and (70):

$$a = -\frac{\mu_2}{\mu_1}B\coth(B) \tag{71}$$

$$a = -\frac{\mu_2}{\mu_1}B\tanh(B) \tag{72}$$

$$a^2 = B^2 + V^2 \tag{73}$$

We can now find the numerical solutions for the modes graphically. At first we will consider the DPS situation where $\varepsilon_1 = \mu_1 = 1$ and $\varepsilon_2 = \mu_2 = 2$, the graphical solution is shown on Figure 12, where the horizontal positive semi-axis represents the transverse propagation constant b and the negative semi-axis represent its imaginary value, that we have previously called B.

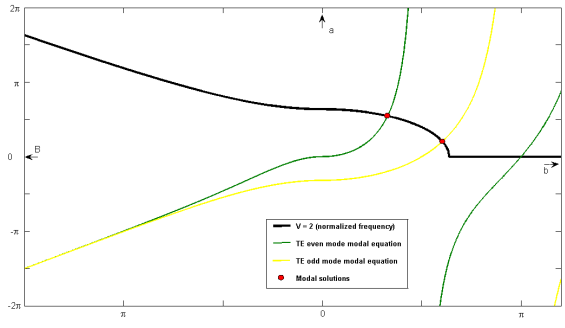

Figure 12. The representation of the modal solutions (red dots) given by the intersection of the curves for a DPS slab with $\varepsilon_1 = \mu_1 = 1$ and $\varepsilon_2 = \mu_2 = 2$.

On Figure 13 we have the modal solution's representation, but now considering a DNG slab with $\varepsilon_1 = \mu_1 = 1$ and $\varepsilon_2 = \mu_2 = -1.5$.

As we can see from the Figures 12 and Figure 13, for the DNG slab there are also solutions with imaginary values of b, that we defined as B. These modes are called **super-slow modes**, since the phase velocity, given by $v_p = \frac{\omega}{\beta}$, assumes such values that:

$$v_p < \frac{c}{\sqrt{\varepsilon_2\mu_2}} \tag{74}$$

The graphical solution for a different value of V is shown in Figure 14.

Form Figure 14 we can also see positive modal solutions, with b being real, as we have seen on the DPS slab, represented on Figure

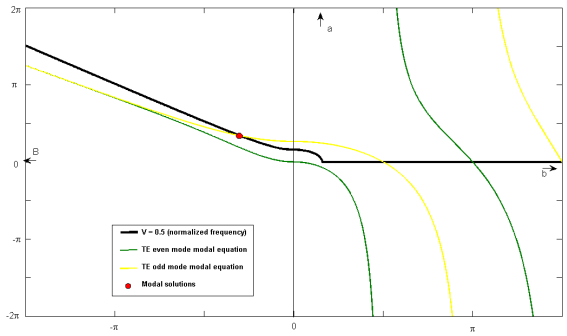

Figure 13. The representation of the modal solutions (red dots) given by the intersection of the curves for a DNG slab with $\varepsilon_1 = \mu_1 = 1$, $\varepsilon_2 = \mu_2 = -1.5$ and $V = 0.5$

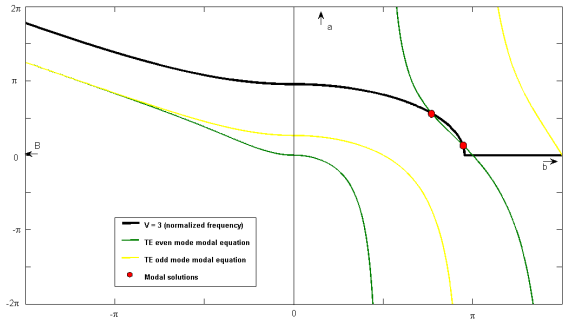

Figure 14. The representation of the modal solutions (red dots) given by the intersection of the curves for a DNG slab with $\varepsilon_1 = \mu_1 = 1$, $\varepsilon_2 = \mu_2 = -1.5$ and $V = 3$

12. These positive-b surface modes are called **slow-modes** since the value of the phase velocity assumes values on the interval:

$$\frac{c}{\sqrt{\varepsilon_2\mu_2}} < v_p < \frac{c}{\sqrt{\varepsilon_1\mu_1}} \tag{75}$$

Since we are now dealing with a DNG medium for the slab, $\varepsilon_2, \mu_2 < 0$, this inverses the signal of the modal equations in such way that the slopes of the tangents and cotangents are changed, and we also have some slow-modes that, for a given range of frequencies, can have more than one solution for the same $h_1 d$ value, as we can see on Figure 14. The representation of the dispersion diagram for the DNG dielectric slab, shown on Figure 15.

Here we can see the two dashed lines that represent transition limits defined by functions of $\beta d(k_0 d)$. The first one, given by $k_0 d = \frac{\beta d}{\sqrt{\mu_1 \varepsilon_1}}$, represents the cutoff condition of the surface modes on the slab, where $h_1 d = 0$. The second limit line, from the relation $k_0 d = \frac{\beta d}{\sqrt{\mu_2 \varepsilon_2}}$, gives us the transition border from a slow-mode to a super-slow surface mode, as we can see from Figure 15 where the fundamental mode is a super-slow odd mode represented by a red curve. This super-slow mode, from Figure 14, becomes a slow-mode when $V = \frac{\mu_1}{|\mu_2|}$ and propagates until $V = \frac{\pi}{2}$ as we can see from Figure 15. On this DNG slab structure we can conclude that there is a direct relation between the constitutive parameters and the resultant dispersive diagram, as the point from which the fundamental mode transitions from a super-slow mode to a slow-mode depends on the value of both μ_1 and μ_2. On the previous situation, that we have used to generate the results on both Figure 14 and Figure 15, we have assumed that $\mu_1\varepsilon_1 < \mu_2\varepsilon_2$ and that $\mu_1 < |\mu_2|$, however, if

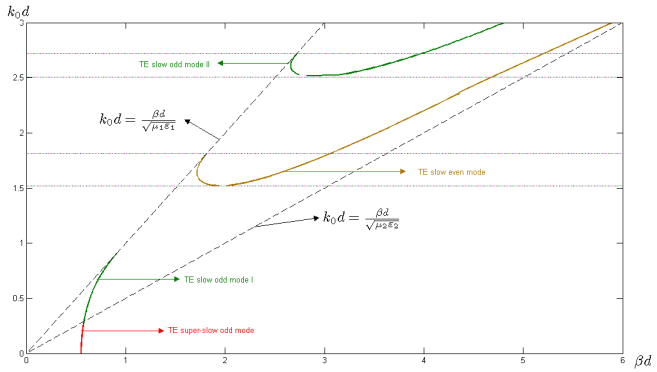

Figure 15. Dispersion diagram for a DNG slab with $\varepsilon_1 = \mu_1 = 1$ and $\varepsilon_2 = \mu_2 = -1.5$

we consider a case where the slab's inner medium is less dense than the outer medium, $\mu_1\varepsilon_1 > \mu_2\varepsilon_2$, we obtain different and important results. From the expression (71) where we defined the normalized frequency, we can easily find that if we consider $\mu_1\varepsilon_1 > \mu_2\varepsilon_2$ we obtain:

$$V^2 < 0 \tag{76}$$

From this result, and still considering the situation where the outer medium is more dense than the slab's inner medium, we have from (70) :

$$b^2 + a^2 < 0 \tag{77}$$

Considering that, in order to have propagation one must satisfy the condition:

$$a^2 \geq 0 \tag{78}$$

So now we can conclude that the following relation must be verified in order to have propagation on the slab:

$$b^2 < 0 \tag{79}$$

These conditions can only be true if we are in the presence of super-slow modes, as we can see from Figure 16, which verify (79) , (80) and $B^2 + V^2 \geq 0$. From this result we can say that the propagation on less dense interior medium, as stated by the inequality (77), is only possible if we are in the presence of super-slow modes and this is a phenomenon that is verified when using a DNG slab. We will now analyze the dispersion diagrams for this situations but considering the influence of the constitutive parameters, as we have mentioned before. As we have done for the denser inner medium, we will first consider the case where $|\mu_2| > \mu_1$. The dispersion diagram is shown in Figure 17.

Here we can see that there is propagation of two super-slow modes where, as we increase in frequency, or $k_0 = \frac{\omega}{c}$, both transverse propagation constants, β tend for the same value. Both these modes have a null cutoff frequency, one being a conventional mode, the even one, and a limited odd mode. The dispersion diagram where $|\mu_2| < \mu_1$ is shown on Figure 18 in order to compare with the results obtained in Figure 17.

On this situation we can see that only one even super-slow mode propagates and on a limited frequency band. We can also notice that, for all the frequency band in which the mode propagates, there are always two modal solutions and these tend to the same value as we increase the frequency. The point where the double-solutions intersect

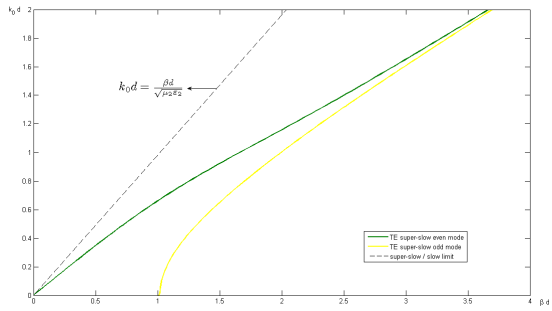

Figure 16. Dispersion diagram for a DNG slab with $\varepsilon_1 = 2$, $\mu_1 = 1$, $\varepsilon_2 = -1$ and $\mu_2 = -1.5$

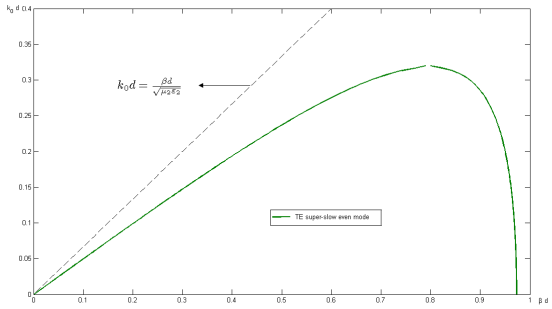

Figure 17. Dispersion diagram for a DNG slab with $\varepsilon_1 = 2$, $\mu_1 = 2$, $\varepsilon_2 = -1$ and $\mu_2 = -1.5$

represents the limit from which there is no surface mode propagation on the DNG slab.

IV. Lens Design Using DNG Metamaterials

Let us consider that there are light rays emanating from a source at point O and that they are being transmitted in the θ direction. In order to convert these light rays to plane waves we must use a lens to assure that the optical paths for the different directions are equal as they reach a plane wavefront. This can be represented by Figure 18.

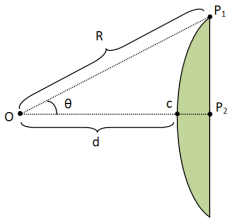

Figure 18. Lens contour and optical path representation

Considering a plane wavefront defined by the line formed with points P_1 and P_2, we can state that the two optical paths must be equal. This equality can be represented by the following expression:

$$\overline{OP_1} = R = \overline{OC} + n\overline{CP_2} \tag{80}$$

Or in polar coordinates:

$$R = d + n[R\cos(\theta - d)] \tag{81}$$

Where n is the refraction index of the material of the lens. Also from Figure 18 we can establish the Cartesian coordinates:

$$\begin{cases} x = \frac{R}{d}\cos(\theta) \\ y = \frac{R}{d}\sin(\theta) \end{cases} \tag{82}$$

Where,

$$\frac{R}{d} = \sqrt{x^2 + y^2} = \frac{1-n}{1 - n\cos(\theta)} \tag{83}$$

From expression (85) we can also establish a direct relation between the coordinates and only the refraction index:

$$\sqrt{x^2 + y^2} = \frac{1-n}{1 - n\frac{x}{\sqrt{x^2+y^2}}} \tag{84}$$

And after some algebraic manipulation:

$$\left(x - \frac{n}{n+1}\right)^2 - \frac{y^2}{n^2-1} = \frac{1}{(n+1)^2} \tag{85}$$

From this expression we can achieve the lens contour in order to verify the equality we have shown in (81). We can also see that expression (86) is in fact an elliptical formula, which degenerates on a circumference as the refractive index approaches $n = 0$. In a matter of fact the 2D lens contours are also commonly called as "circles" [3]. Different lens' contours, for different values of n, are represented in Figure 19.

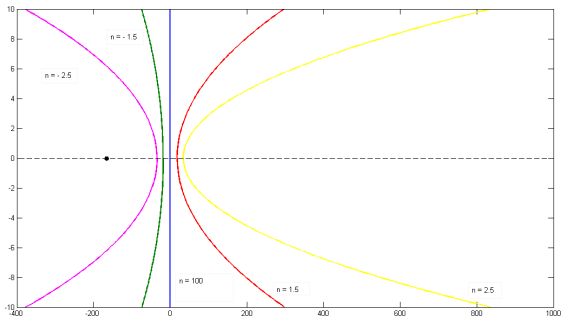

Figure 19. The lenses contours for different refraction indexes, $n = -2.5, -1.5, 100, 1.5, 2.5$

From (82) we can see that there is an asymptote in $n = \frac{1}{\cos(\theta)}$, making the contours hyperbolic. We can also see from Figure 19 that the curvature is the opposite depending on n being either positive or negative.

After we have calculated the optical path we can now analyze the design in terms of focal length. It can be given, as f, by the following expression:

$$f = \left|\frac{R_c}{1-n}\right| \tag{86}$$

From this expression we can see that this length depends on the refractive index, n, and the radius-of-curvature of the lens surface, R_c. So, if we consider n to be negative, a lens with that properties can alter the trajectory of transmitted waves as if the material possessed a much larger positive index.

V. The Veselago's Flat Lens

As we have seen from the expression (86) and in Figure 19, as the refraction index tends to large values (or even infinity), the contour tends to a straight line, which can be called as a "flat lens" [3]. Knowing that such a large refractive index does not have any important practical application [3], a functional "flat lens" was proposed by Victor Georgievich Veselago in 1968 [4]. In Veselago's paper [4] he proposed that a plannar slab, composed by a material with the refractive index $n = -n_0$, with n_0 being the refractive index of the medium in which the slab was immersed, would focus the light waves emited by a source to a single point. This can be showed by a simple aplication of Snell's law, using a structure with two consecutive boundaries. This structure is called the Veselago's flat lens [3] and a graphical representation is shown in Figure 20.

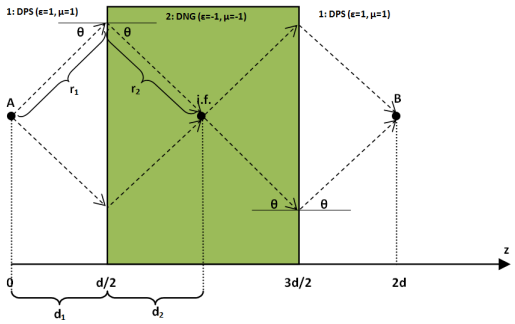

Figure 20. Passage of light waves through a Veselago flat lens, **A**: the image source, **B**: focused image, **i.f.**: the internal focus point

This lens' geometry and structure, which converts a diverging beam to a converging one, and vice-versa, creates the existance of a particular point called the internal focus, represented in Figure 20. Knowing that the optical path from the external focus point to the internal focus point must be zero, we can also processd to the computation of the lens contour, as we have done in the previous section. From Figure 20 we can state that, in order to have an equallity of optical paths, one must have:

$$r_1 + nr_2 = d_1 + nd_2 \tag{87}$$

$$r_2^2 = r_1^2 + (d_1 + d_2)^2 - 2r_1(d_1 + d_2)\cos(\theta) \tag{88}$$

where, n is the refractive index of the lens. Assuming that the optical path from focus to focus is zero one must have:

$$d_1 + nd_2 = 0 \tag{89}$$

In polar coordinates, after some manipulation:

$$(n+1)\left(\frac{r_1}{d_1}\right)^2 - 2n\cos(\theta)\left(\frac{r_1}{d_1}\right) + (n-1) = 0 \tag{90}$$

As done in (83), using the Carthesian co-ordinates we obtain the following equation for the lens contour:

$$\left(x - \frac{n}{n+1}\right)^2 + y^2 = \frac{1}{(n+1)^2} \tag{91}$$

Which is the expression of a circumference centered at $\left(\frac{n}{n+1}, 0\right)$, and when $n = -1$ we also obtain a flat lens. The equality imposed by expression (90) clearly implies that one must have a NIR medium, which include all DNG media.

Let us now consider the general expression for the impedance of a specific medium:

$$Z = \sqrt{\frac{\mu_0\mu}{\varepsilon_0\varepsilon}} \tag{92}$$

If we consider that the slab's material has, for the relative permittivity and permeability, both $\varepsilon_r = \mu_r = -1$, we can state that this DNG medium is a perfect match to free space ($\varepsilon_{0r} = \mu_{0r} = 1$). From this result, one of the conclusions is that there will not be reflections at the interfaces between the lens and freespace and even at the far boundary interface there is again an impedance match, and the light is again perfectly transmitted to vaccum.

If the propagation is done in the $\widehat{z}$ axis, in order to have all the energy transmitted throught the slab it is required that we have a propagation constant:

$$k'_z = -\sqrt{\frac{\omega}{c^2} - k_x^2 - k_y^2} \tag{93}$$

With the overall Trasmission coefficient being:

$$T = tt' = \exp(ik'_z d) = \exp\left[-i\left(\sqrt{\frac{\omega}{c^2} - k_x^2 - k_y^2}\right)d\right] \tag{94}$$

where d is the thickness of the slab. The choice of the propagation constant is done in order to maintain causality and this phase correction is what grants the lens the capability of refocusing the image by canceling the phase of the transmitted wave as it propagates from its source [4].

Let us consider a TE wave propagating in the vaccum, medium 1, with the following field expression:

$$E_1 = \exp(ik_z z + ik_x x - i\omega t) \tag{95}$$

where the propagation constant is:

$$k_z = i\sqrt{k_x^2 + k_y^2 - \frac{\omega^2}{c^2}} \tag{96}$$

with $k_x^2 + k_y^2 > \frac{\omega}{c^2}$. From this field expression in (97) we can easily identify that we are dealing with an exponentially evanescent field. It is also important to notice that in order to maintain causality the fields must decay as the get away from the interface, so the field expression for the transmitted wave can be:

$$E_{t2} = t\exp(ik'_z z + ik_x x - i\omega t) \tag{97}$$

And for the reflected wave, the following expression:

$$E_{r1} = r\exp(-ik_z z + ik_x x - i\omega t) \tag{98}$$

where the propagation constant is given by:

$$k'_z = i\sqrt{k_x^2 + k_y^2 - \varepsilon_2\mu_2\frac{\omega}{c^2}} \tag{99}$$

with ε_2 and μ_2 being the permittivity and permeability of the slab, and also having $k_x^2 + k_y^2 > \varepsilon_2\mu_2\frac{\omega}{c^2}$.

When matching the wave fields at the interface from medium 1 to medium 2 we obtain the reflection and transmission coefficients, t and r:

$$t = \frac{2\mu k_z}{\mu k_z + k'_z} \tag{100}$$

$$r = \frac{\mu k_z - k'_z}{\mu k_z + k'_z} \tag{101}$$

And for the transmission and reflection coefficients of the transition from inside medium 2 to medium 1:

$$t' = \frac{2k'_z}{\mu k_z + k'_z} \tag{102}$$

$$r' = \frac{k'_z - \mu k_z}{k'_z + \mu k_z} \tag{103}$$

Now in order to obtain the expression for the transmission of light throught both the interfaces one must sum the multiple scattering events, from [5]:

$$T_s = tt' \exp(ik'_z d) + tt' r'^2 \exp(3ik'_z d) + tt' r'^3 \exp(5ik'_z d) + (...) \tag{104}$$

$$T_s = \frac{tt' \exp(ik'_z d)}{1 - r'^2 \exp(2ik'_z d)} \tag{105}$$

Considering the DNG situation (with $\varepsilon = \mu = -1$), and using (101)-(106), we can compute the limit to this values of permitivity and permeability in order to find the overall transmission coefficient. The solution for this special kind of structure is calculated asymptotically as n aproaches -1:

$$\lim_{\mu \to -1, \varepsilon \to -1} (Ts) = \exp(ik'_z d) = \exp(ik_z d) \tag{106}$$

This result in (107) is very important. As another consequence of having a negative index of refraction, we have waves of the form $\exp(-k_z)$, outside the lens, that couple to waves of the form $\exp(k_z)$ inside the lens. So, even if the waves decay outside the lens, they are *ńamplifiedż* on the inside of it, recovering an image on the opposite side of the lens, from the source, and all done by the transmission process. On Figure 21 we can see the evolution of the evanescent field variation in the presence of the Veselago's flat lens.

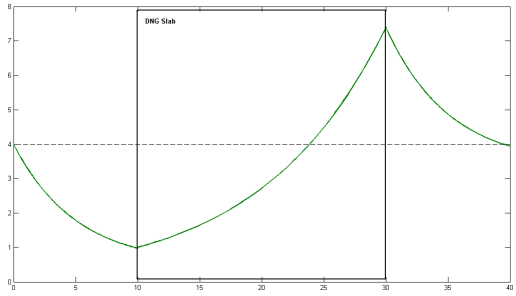

Figure 21. Evanescent field variation in the presence of the Veselago's flat lens.

Since the waves decay in amplitude and not in phase, as they get further from the source, the lens focus the image by amplifying these waves rather than correcting the phase. This is a proof that this medium does in fact amplify the evanescent waves, and so, with this kind of lens, both the propagating and evanescent waves contribute to the resolution of the resulting image [5].

As we have stated before, as the result of the perfect matched impedance, there will be no reflected wave on the interface as we can also see by the assymptotic analysis of the overall reflection coefficient:

$$\lim_{\mu \to -1, \varepsilon \to -1} (Rs) = 0 \tag{107}$$

Which confirms that all the energy is trasmitted between the media transitions.

VI. Conclusions

We have shown that in this kind of media the existence of waves that propagate in a antiparalell direction of the power flux is noticed, called the Backward Waves, and that we are in the presence of a Negative Index of Refraction material, which implies some modifications in the interpretation of Snell's Law. From the introduction of losses we have also concluded that both the group and phase velocities have different values and, for this kind of DNG media, they even have opposite directions.

We have also chosen to study two simple structures, the DPS-DNG interface and te DNG slab. First we have showed that it is possible to have both TE and TM surface mode wave propagation on a DPS-DNG interface. This kind of propagation mode is new and does not exist in other more conventional DPS wave guiding structures. When dealing with the propagation of this surface waves we have also seen that it permits large attenuation outside the interface. Finally we have analyzed the guided propagation on a DNG slab. In this structure there's also the possibility of having surface wave mode propagation but the most important result is the propagation of super-slow modes that are a consequence of having a phase velocity that is smaller than the outer medium in which a DNG slab is immersed (there is also slow-mode propagation that exhibits a double modal solution for some frequency bands). The existence of these super-slow modes enables the propagation on the DNG slab even if we use a less dense medium for the slab (i.e., medium 2) when compared to the outer medium (i.e. medium 2), $\varepsilon_1 \mu_1 > \varepsilon_2 \mu_2$.

Finally we have studied the lens design using DNG metamaterials. In order to do so we have studied the situation where a DNG slab is used in order to produce an high resolution lens, which is called the Veselago's flat lens. From the concept of optical path we have obtained an expression that enables us to infere about the geometrical form of the lens contour and about its dependance on the value of the refractive index of the lens' material. The curvature of the lens contour can be concave if we are dealing with positive refraction indexes and convex if we are dealing with negative refraction index materials. The concept of focal lenght is also introduced into the lense design and we have seen that for a lens made of a DNG material, we can obtain the same focal lenght as we would if a DPS material was used, but with the implication of having a much smaller refraction index. Then we introduced the Veselago DNG flat lens. When considering that the lens's material has, for the relative permittivity and permeability, both $\varepsilon_r = \mu_r = -1$ we could see that there was a perfect impedance match for both interfaces between the DNG slab and the medium in which it was immersed and one of the conclusions is that there will not be reflections at the interfaces between the lens and free space and even at the far boundary interface and the light is again perfectly transmitted to vaccum to a single point. The DNG material properties creates a physical phenomenon where we have waves of the form $\exp(-k_z)$, outside the lens, that couple to waves of the form $\exp(k_z)$ inside the lens. So, even if the waves decay outside the lens, they amplified inside of it, recovering an image on the opposite side of the lens, from the source.

VII. References

References

[1] C. R. Paiva. Introdução aos metamateriais. 2008.
[2] R. Ziolkowski N. Engheta. *Metamaterials: Physics and Engeneering Explorations*. Addison-Wesley, 206.
[3] Ekaterina Shamonina Laszlo Solymar. *Waves in Metamaterials*. Oxford University Press, USA, 2009.
[4] V. G. Veselago. The electrodynamics of substances with simultaneously negative values of ε and μ. *Soviet Physics USP*, 47, 1968.
[5] J. B. Pendry. Negative refraction makes a perfect lens. *Phys. Rev. Lett.*, 85, 2000.